Contents lists available at ScienceDirect

Optics and Lasers in Engineering

journal homepage: www.elsevier.com

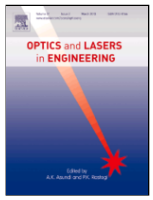

Review

A descriptor of speckle textures using box fractal dimension curve

H. Rabal[a, *], E. Grumel[a, b], N. Cap[a], L. Buffarini[a], M. Trivi[a, b]

[a] Centro de Investigaciones Opticas, CIOp (CONICET – UNLP – CIC), P.O. Box No. 3, 1897 Gonnet-La Plata, Argentina
[b] UIDET OPTIMO, Departamento de Ciencias Básicas, Facultad de Ingenieria, Universidad Nacional de La Plata, La Plata, Argentina

ARTICLE INFO

Keywords:
Box fractal dimension
Speckle
Dynamic speckle
Textures
Roughness
Ultrasound images

ABSTRACT

We propose a simple generalization of the box fractal dimension in images by considering the curve obtained from its value as a function of the binarization threshold. This curve can be used to partially describe ordinary images, textures, static and dynamic speckle patterns. We show some examples of different applications of this approach in some cases of interest.

1. Introduction

Rough surfaces illuminated by coherent laser light show a grainy appearance called speckle [1–2]. Speckle techniques have been applied to study different experimental situations. According to the problems to be solved, different algorithms are required, for example, speckle correlation to study surface roughness [3] and digital speckle pattern interferometry (DSPI) for the study of displacements, deformations and cracks [4].

When the surface changes, its speckle pattern also changes and it is called dynamic speckle [5]. Some properties of the surface changes can be inferred from the time dynamics of its irradiance. Several applications of the measurement of dynamic speckle activity have been found in medicine, biology, industry, agriculture, etc. [see 5 and references therein]. Also, some algorithms have been developed for different applications. In general, the algorithms used in these techniques are useful to solve some situations but cannot be applied to others. For example, when we try to describe static or dynamic speckle patterns it is very difficult to find a single algorithm to analyze both situations.

In a recent work we performed an exhaustive comparative analysis of the descriptors most often used in different applications [6].

Also, we have proposed and shown the possibility to apply the box fractal dimension to characterize speckle patterns in some restricted situations [7]. In that case, we showed numerical simulations and a controlled experiment.

Fractal dimensions, introduced by B. Mandelbrot [8], have been found as useful descriptions in mathematics, in many images such as those that can be found in natural landscapes, patterns, sequences, biological tissues, simple life forms, organic systems, complex life forms, environments and many other branches of the natural sciences.

In this paper, we propose to extend the use of the box fractal algorithm to characterize both static and dynamic speckle patterns in several experimental situations, but it can also be applied to other types of images. It is possible, with a single algorithm and small adaptations, to apply it to very different problems.

We present the results on laser static speckle patterns in an example of roughness and on dynamic speckle quantitative measurements for free propagation geometry in controlled experimental conditions, in the evolution process of polymers (drying of paint) and in ultrasound speckle images.

2. Theory

2.1. Box fractal dimension

The box fractal dimension (BFD), also named the box counting dimension or similarity dimension, is a method of characterizing data, for example, curves or binary images, by decomposing the subject into boxes (usually squared) of different sizes and measuring how the data cover the plane at different scales [8]. If the image is not binary, it must binarized using some threshold U_0 so that every pixel of the image is set to 0 if its value is smaller than U_0 and to 255 in other cases.

The box fractal dimension for that threshold is obtained using the expression:

$$N(s) = B.s^{-BFD} \tag{1}$$

* Corresponding author.
Email address: hrabal@ing.unlp.edu.ar (H. Rabal)

https://doi.org/10.1016/j.optlaseng.2018.02.006
Received 14 November 2017; Received in revised form 5 February 2018; Accepted 10 February 2018
Available online xxx
0143-8166/

where s is the size of the side of each square box, B is a constant, $N(s)$ is the number of boxes with side s required to cover the image and BFD is the box fractal dimension. In the limit $s \to 0$.

As images are only accessible as discrete integer numbers, the limits $s \to 0$ cannot be reached. Then, in practice, the BFD is estimated as the slope of the straight line best fitting (least square error) a log–log graph:

$$-(\log N(s) \text{ vs } \log s) \tag{2}$$

for a series of different values of s.

We are going to use an example to illustrate the procedure:

a) A grid is overlaid on the two-dimensional binary image of an object with grid size = $s \times s$ as shown in Fig. 1.
b) Then $N(s)$, the number of cells containing at least one white point of the object, is counted and stored. The number of cells containing at least one dark point could alternatively be used.
c) Next, the size of the grid $s \times s$ is changed and the process repeated.
d) With the obtained results, log (N (s)) is plotted versus log (s). See Fig. 2.
e) The best fitting straight line is determined by using minimum squares. Its slope with reversed sign is, by definition, the box fractal dimension (BFD) estimation for every chosen binarization threshold U.

The original image is again binarized with a new U threshold value. The BFD measurement is then repeated on the result.

Changing the value of U generally produces a different value for the BFD. There seems to be no unique criterion for the choice of the optimum threshold value in all cases. In digital image processing there are several thresholding techniques used to binarize images. Two popular thresholding criteria are to use the middle value of the dynamic range and the Otsu method [9].

It is possible that for some unfortunate choice of the threshold two or more experimental situations result in the same or close value for the fractal dimension, making it impossible to distinguish between them (see for example Figs. 12a and 13a below). For these cases, it is convenient to use more than one threshold value.

B. Chaudhuri and N. Sarkar [10] proposed an improved method for the calculation of the fractal dimension, named Differential Box Counting. In it, although there was no explicit use of a threshold, the dynamic range inside each box was used to count the number of occupied ones for the calculation of the FD. That procedure was used, for example, for segmentation of textures [11] and several improvements were proposed afterward [12–14]. The use of all possible thresholds was not contemplated because for very high values of the threshold very few points are left and the adjustment of the calculation is very poor.

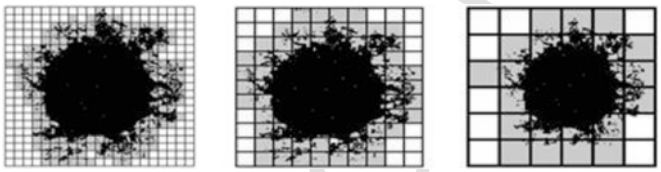

Fig. 1. A red wine drop on paper and how it is covered with three different grids.

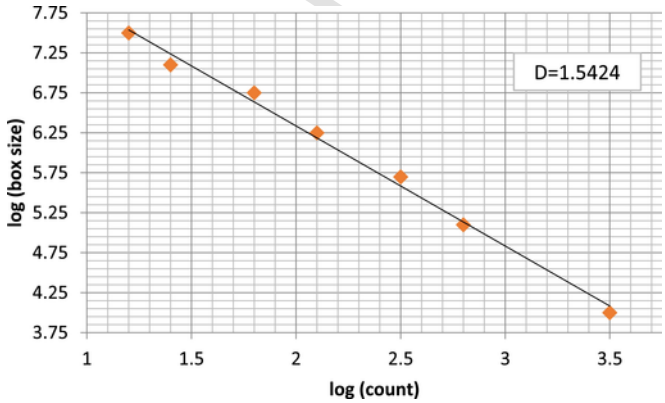

Fig. 2. log (N (s)) plotted versus log (s).

Nevertheless, complex textures could include different structures with different fractal dimensions in different ranges of the image's dynamic range.

In the Chaudhuri and Sarkar method, the image is considered as a surface in a 3D space divided into boxes, with the intensity at each pixel as the third coordinate. Boxes are counted considering the maximum and the minimum value of intensity in the contained volume. This so defined dimension is then a single value between 2 and 3. No other threshold is considered.

In this work, we propose the use of all possible values of U so that information on structures with different gray levels can be preserved. We call this result the box fractal dimension curve (BFDC).

In this approach, each thresholded image is equivalent to a level cut of the surface defined in Sarkar's method and projected on the x, y plane. So, when every possible threshold is considered, a set of numbers between 0 and 2 are obtained. By continuously changing the threshold, the obtained box fractal dimension describes a curve that is characteristic of the distribution of gray levels in the image.

Theoretically, the curve should start with the value 2. In practice, nevertheless, when the curve is numerically adjusted, the result may be slightly higher or lower than the theoretical value. This is due to the error committed when the image is quantized. By increasing the number of bits this undesired effect can be alleviated.

2.2. Box fractal dimension curve (BFDC) in an image example

As a first step to illustrate the use of the BFDC algorithm, in this section we show its application to the well-known case of the mandrill image.

A digital image in incoherent light is an array of integer values, named gray levels, distributed on a bidimensional frame. Each value represents the irradiance registered on the sensitive plane of a camera. As irradiance is usually a continuous function of the position, a quantization of its values and a spatial sampling are inherent to the register [15]. The distribution of the gray levels can be visualized by its histogram.

One frequent operation in image processing is binarization. It consists in segmenting the image according to comparison of the gray levels with a threshold value. If the gray level of a pixel is higher than the threshold, the binarized image is assigned the highest value (usually 255) and the rest is assigned to be zero. The binarization operation generates a sharp, usually irregular, edge between the bright and the dark regions.

In this work we explore the use of the fractal dimension of that binarized image as a function of the chosen binarization threshold. It is evident that if the threshold is very low, most of the pixels in the binarized image are going to be bright and cover a substantial area of the image. It is to be expected that in that case the fractal dimension will be near the value 2. Conversely, when the threshold value is higher than the highest irradiance pixel value, all the binarized image will be uniformly black and the fractal dimension will be zero. Between these extreme situations, the fractal dimension as a function of the threshold will describe a curve that we name the box fractal dimension curve (BFDC).

Fig. 3a) shows a typical example image of a mandrill used in many image processing examples. Fig. 3b) shows the histogram of the image. Fig. 3c) shows the result of applying the concept of the box fractal dimension curve (BFDC) to the image of the mandrill. Notice that it starts at 2, that is, for small thresholds the binarized image covers all of the plane. This is so until the threshold reaches the smallest occupied value of the histogram (22 in Fig. 3b). Then, it decreases, in this case almost monotonically, to 0 for the highest occupied level and over. Between these two values, the particular behavior of the curve depends on the characteristics of the image.

This is so when the image has a histogram where all possible gray levels are occupied between the minimum and the maximum.

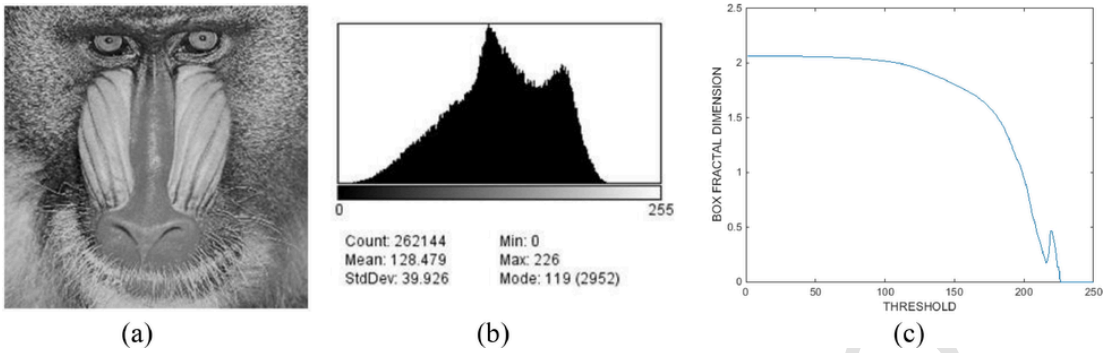

Fig. 3. a) Image of mandrill, b) histogram, c) box fractal curve.

Alternatively, images are often compressed for transmission or storage of only the visually relevant features. That is, only some gray levels are present, intending to preserve the visual quality. Fig. 4a) shows a compressed version of the mandrill image and Fig. 4b) its discrete histogram, which shows that only some gray levels are present in the compressed image. Fig. 4c) shows the box fractal dimension curve (BFDC) of the compressed image of the mandrill. The change of the threshold in the absent intervals does not change the value of the measured dimension and the curve then shows a stepped aspect.

Something similar occurs if the image contains saturated regions. The curve is horizontal in these regions.

One advantage of the curve is the following: As two different images may lead to different BFDCs, they eventually cross and this fact makes evident that the wrong choice of a single threshold can induce the wrong conclusion that both images bear the same fractal properties. After the two BFDCs are compared, regions of thresholds where discrimination is better can be apparent.

2.3. Box fractal dimension curve (BFDC) in speckle pattern images

When the images are obtained using coherent illumination and the scene is optically rough, a speckle phenomenon is present. It appears mostly as a multiplicative high contrast granular noise with statistically almost random distribution that degrades the image quality. This is due to the interference between scattered wavelets in the roughness height variations with random optical path differences. When the scattering centers present in the object are mutually independent and their phases are uniformly distributed in the $[-\pi, \pi]$ interval, the contrast of the speckle pattern is 1 and it is said to be "well developed" [16].

Next, we are going to consider the box fractal dimension curve method in speckle patterns images for several situations.

When speckle images are obtained by free lensless propagation from the object to the detector, this is named objective speckle and, in principle, every pixel of the image receives contributions from all the points of the object. As the irradiance in all points of the image is representative of the statistical properties of the diffusing object, then a BFDC can be obtained as described before.

Fig. 5 shows an image of a) an objective speckle pattern and b) a threshold binary image obtained from it. Fig. 5c) shows the BFDC of the speckle pattern. The BFDC in this case represents a quantitative description of how the gray levels are distributed and cover the image plane.

As the histogram of a well-developed speckle pattern contains a continuous distribution of gray levels, the curve does not show steps but is also a continuous curve.

It starts near the value 2 for low thresholds and then decreases at a rate that depends on the surface roughness of the illuminated sample and finishes near zero for high values of the threshold. Theoretically, it should start exactly at the value 2. Actual calculations usually show a small difference. Notice that for high values of the threshold the curve shows an irregular behavior. So, when the threshold is very high, the number of points with intensity higher than that value is very small and the box counting procedure becomes erratic and not reliable. Those values were not taken into account for the calculations in the rest of this work.

2.4. Effect of the number of boxes employed

Due to limited resolution, in Nature there are no patterns that are fully fractal. They may exhibit only an approximate fractal behavior for certain intervals of the scaling. To check if an image can be described as quasi fractal, we show here (Fig. 6) the goodness of the fit for its r^2 of the log–log plot to a straight line for a speckle pattern. This graph shows that value for a speckle pattern as a function of the binarization threshold for five and nine boxes. In this case, it can be seen that up to the threshold value of 75 the fit is very accurate for both five and nine boxes. Then, for the threshold value up to 150 the fit is good for five boxes but decreases to about 0.9 for nine boxes. This value is an indication of the range within which the pattern behaves as an approximate fractal within a chosen tolerance.

2.5. Approximation with the Fermi–Dirac (FD) distribution

Even if the following approximation is not true for the general case, the BFDC is often a sigmoidal accumulative function. For some cases of dynamic speckle images, it can be successfully fitted with the function of the threshold

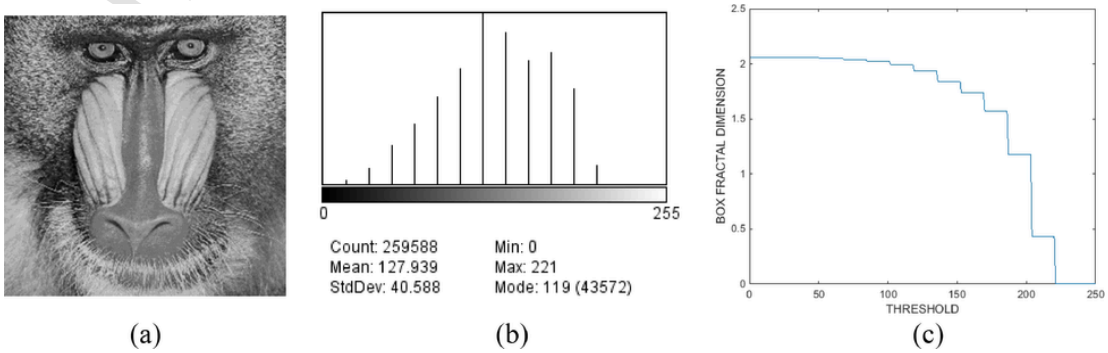

Fig. 4. a) Compressed image of mandrill, b) histogram, c) box fractal curve.

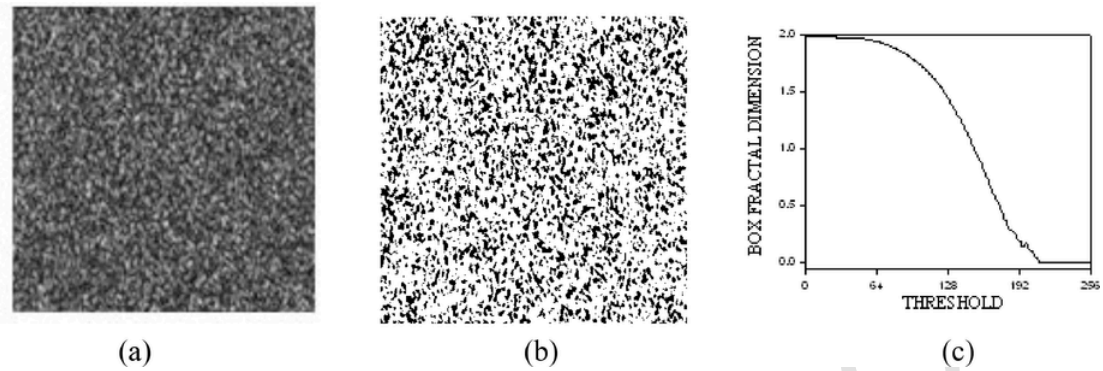

Fig. 5. a) Speckle pattern, b) binarization of a), c) box fractal curve.

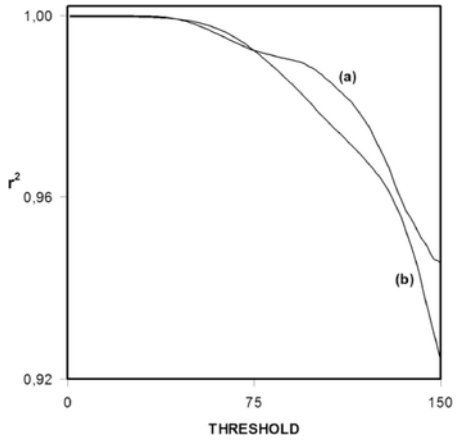

Fig. 6. Goodness of the fit r^2. a) Five boxes, b) nine boxes.

U:

$$BF(U) = \frac{A}{1 + \exp\left(\frac{U - U0}{T^*}\right)} \tag{3}$$

This expression is similar to the Fermi–Dirac (FD) statistical distribution of fermions [17] as shown in Fig. 7, but with $A = 2$ instead of 1 as in FD.

The units of the temperature T^* are the same as those for thresholds, that is, gray levels.

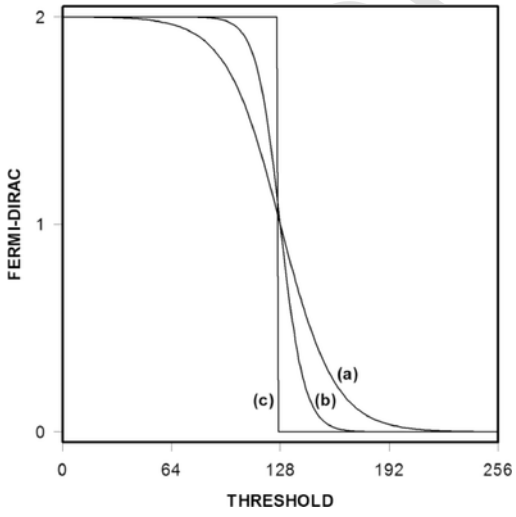

Fig. 7. Plot of Eq. (3), similar to the Fermi–Dirac statistical distribution of fermions, but for $A = 2$. (a) $T^* = 28$, (b) $T^* = 16$, (c) $T^* = 0$.

In our case, for each speckle pattern image we numerically adjust the curve with this expression. A is a constant ($A = 2$) determining the upper asymptote and U_0 a constant that depends on the mean value of the speckle pattern intensity. It corresponds to the Fermi level in quantum statistics and the function value there is $A/2$. T^* is a parameter that plays the same role as the absolute temperature and that describes the rate of change of BF by varying the binarization threshold U. This "fractal temperature" T^* is zero if the original image is binary and the curve is a step function that resembles the zero degree Kelvin plot for fermions. When the fractal temperature T^* is high, the curve tends to be similar to the Boltzmann distribution [18].

For limited but broad intervals of threshold, this fitting is highly accurate. Out of those intervals, for high values of the threshold this approximation breaks and the curve behaves erratically. This is due to the fact that the BFDC is not accurately determined as the log–log plot cannot be successfully fitted to a straight line.

For speckle phenomena behaving in this FD-like way, they can be described in terms of the temperature T^* (named so by analogy). The temperature is measured in the same units as the irradiance in the image.

Now, we are going to find the derivative of the FD curve (Eq. (3)) with respect to the threshold values.

$$\frac{\mathrm{dFD}}{\mathbf{d}U} = \frac{-\frac{A}{T^*}\exp\left[\frac{U - U_0}{T^*}\right]}{\left\{1 + \exp\left[\frac{U - U_0}{T^*}\right]\right\}^2} \tag{4}$$

The derivative is in the shape of a negative lump as shown in Fig. 8 for two different temperatures ((a) $T^* = 28$, and (b) $T^* = 16$). Its width is proportional to the temperature T^*.

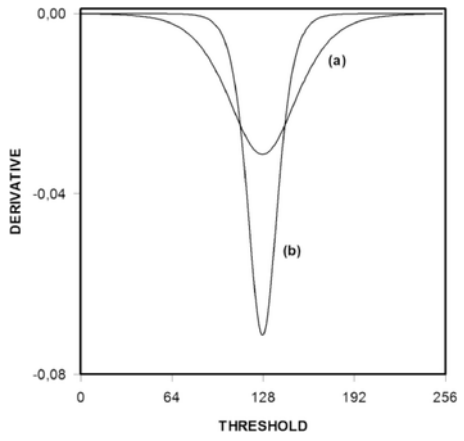

Fig. 8. Plot of the derivative of Eq. (3), the Fermi–Dirac statistical distribution of fermions for two temperatures ((a) $T^* = 28$, and (b) $T^* = 16$).

Then we look for its minimum value that occurs at $U = U_0$:

$$\text{If } U = U_0, \quad \text{then} \quad FD = \frac{A}{2} \tag{5}$$

$$\frac{-FD^2}{AT^*} \exp\left(\frac{U-U_0}{T^*}\right) = \frac{-A}{4T^*} \tag{6}$$

We are going to estimate the half of the minimum value of the derivative. It is found as

$$\frac{-FD^2}{AT^*} \exp\left(\frac{U-U_0}{T^*}\right) = \frac{-A}{8T^*} \tag{7}$$

and it is reached at

$$\exp\left(\frac{U-U_0}{T^*}\right) = 3 \pm 2\sqrt{2} \tag{8}$$

$$U = U_0 + T^* \ln\left(3 \pm 2\sqrt{2}\right) \tag{9}$$

So that the full width at half minimum results in

$$\Delta U = 1,5159\ T^* \tag{10}$$

That is, the temperature analog can be found as the full width at half minimum (FWHM) times a constant. In the limit when T^* tends to zero, a delta distribution is obtained and it corresponds to binary images.

When the fractal curve is the sum of two FD distributions, thus indicating the presence of two phenomena, the derivatives of the curve show it as bumps if the components are fully resolved and overlapped otherwise.

In Fig. 9a) we show the result of numerically adding two FDs after normalization to the 0–2 interval. In Fig. 9b) we show its derivative. In this case the parameters U_0 have been chosen so that the lumps in the derivatives are well resolved.

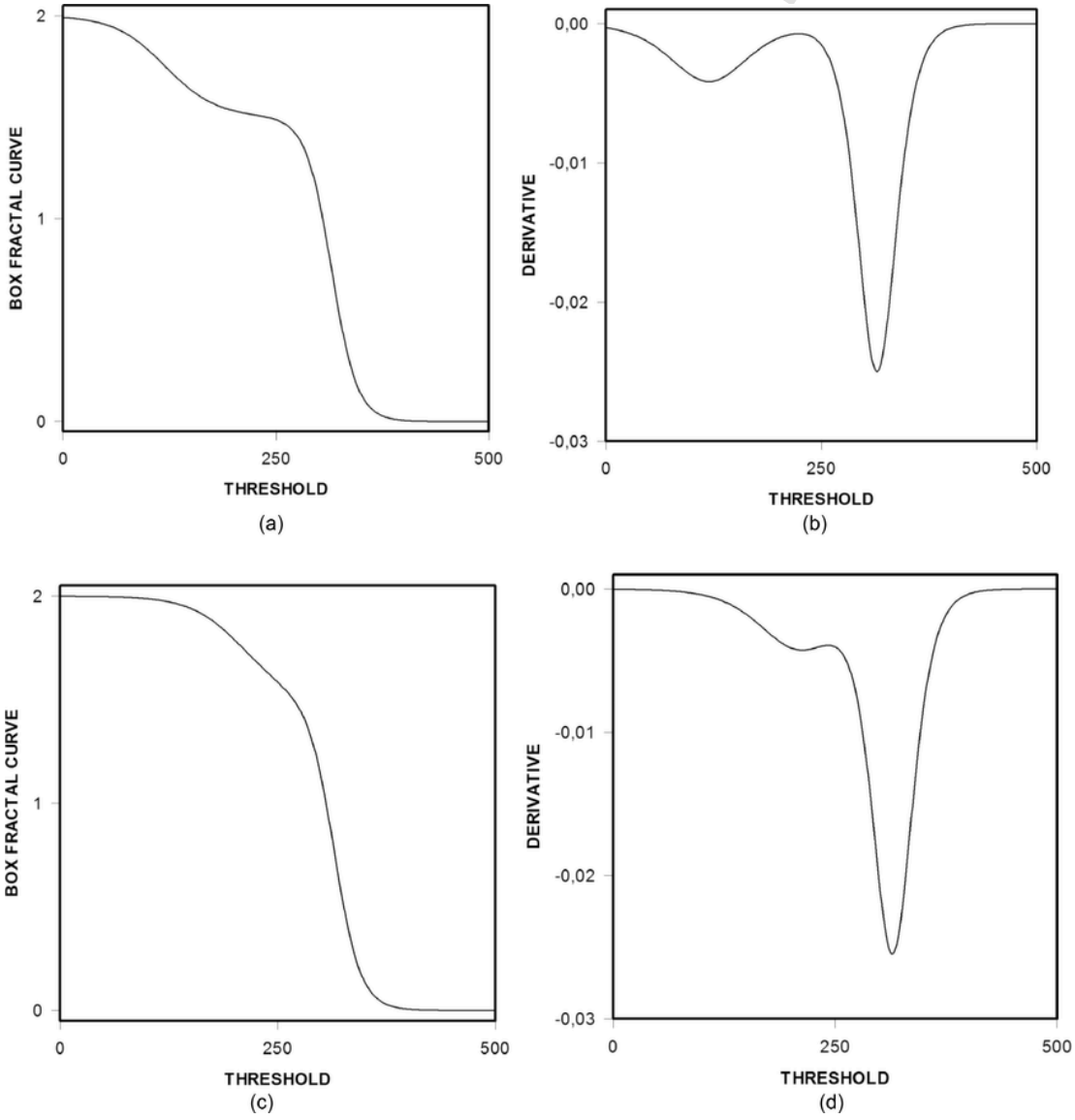

Fig. 9. Box fractal curves obtained as the addition of two FD and their derivatives: Resolved a) and b) and not resolved cases c) and d).

In Fig. 9c) we show a similar profile calculated when the values of U_0 were chosen so that the lumps were not fully resolved, as can be seen in its derivative in Fig. 9d). The term resolved is used here in a similar way as in diffraction and spectroscopy.

It can be seen that when both components are well resolved, their temperatures can be approximated using Eq. (10).

We are going to show a numerical simulated example in the next section.

2.6. Numerical simulated example

We have seen how the width of the derivative of the fractal curve permits the estimation of the temperature of a Fermi–Dirac-like distribution (Eq. (3)).

We have also shown how the sum of two FD in the well resolved case shows two separate lumps in its derivative. Eq. (4) then permits an estimation of their temperatures with a small error if the lumps do not appreciably overlap.

We are going to describe now how this situation can be simulated and shown in practice.

For the simulation, one possibility is to take two frames of different (dynamic or not) situations but with different fractal curves. In what follows we take two different drying states of paint: wet and dry.

We build a synthetic image in the following way: Each pixel of the first frame is assigned the value 0 if it belongs to the right half of its histogram and kept unaltered otherwise. Then this operation is repeated for the second frame, but assigning the value 0 if it belongs to the left half of its histogram and kept unaltered otherwise. Finally we add the obtained images.

In this way we obtain a result where we have forced the fractal curve to show the behavior of one state for low values of the threshold and a different one for the higher values (see Fig. 10). The derivative of this fractal curve then shows a secondary lump as shown before in Fig. 9(a) and (b).

This situation can also be found in some experimental situations. We show an actual experiment in Section 3.2.3.

3. Experimental result

3.1. BFDC on speckle pattern images

The speckle phenomenon, both static and dynamic, has given rise to numerous applications [3–5]. We are going to apply the box fractal dimension curve method developed in Section 2.3 in images of both static and dynamic speckle experiments.

3.1.1. Static speckle pattern: algorithm repeatability test

In this section we are going to apply the proposed algorithm to the most simple speckle situation, such as a single fully developed speckle pattern obtained by free propagation from a plane diffuser to the observation plane.

To standardize the diffuser characteristics, we use a sample with a normalized roughness surface. We tested the BFDC algorithm on still free propagation speckle patterns obtained by illumination of Rugotest Roughness Comparison Specimens. This is a set of metal samples for tactile and visual comparison of a workpiece surface finish according to various machining processes. The specimen sets are made according to individual machining processes (ISO 2632-1 and 2632-2).

Its roughness steps were too big to follow the BFCD performance as a function of some roughness parameters and this was not the main aim of this work. Exploiting the fact that the surface had homogeneous roughness (according to Norm) and it did not change with time, we could test if the BFCD was repetitive using a stable, deterministic and reproducible situation.

The parameters indicated by the Rugotest specifications of the sample used (N1) are:

Ra (arithmetic average roughness) Ra = 0.025 μm.
Rp (geometric average roughness or RMS: root mean square) Rp = 0.05 μm
Rz (mean peak-to-valley height) Rz = 0.16 μm.

We registered images of the speckle patterns generated by illuminating a Rugotest standard plate with the unexpanded He–Ne laser, recorded using a lensless camera.

We tested the BFDC in two perpendicular directions according to the directions of the grooves on the sample: longitudinal and transversal.

Five images on different points of the N1 section were registered by displacing the sample in the direction transversal to the machining of the sample, and five more images in the same direction as the machining.

We calculated the BFDC algorithm for each speckle image and then we used Eq. (3) to calculate the best numerical fit function using the Fermi–Dirac equation. Each fit was characterized by a "fractal temperature" T^* equivalent that describes the rate of change of the box fractal curve.

The curves obtained in the ten measurements and the corresponding temperatures T^* are shown in Fig. 11. It can be seen that the procedure gives different results for the two considered directions. However, notice that in both separate cases, the five curves mostly overlap, showing that the method is fairly repetitive.

3.2. Dynamic speckle patterns

3.2.1. Stepping motor experiment

In this section we explore a more complex situation. In this case, we consider speckle patterns evolving in time.

To verify the performance of the BFDC algorithm applied to dynamic speckle patterns, we tested a case with a controlled experiment in translation condition [18–19].

The optical set-up was described in the references. An attenuated 10 mW He–Ne laser was used to illuminate the object plane. A CCD camera Pulnix

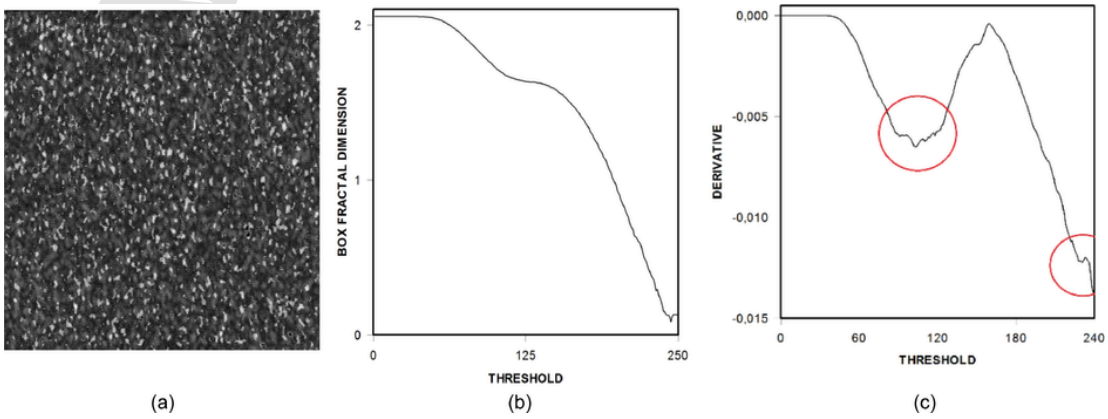

Fig. 10. a) Synthetic image, b) box fractal curves of the synthetic image, c) derivative of BFDC of b). The circles indicate the two lumps (negative).

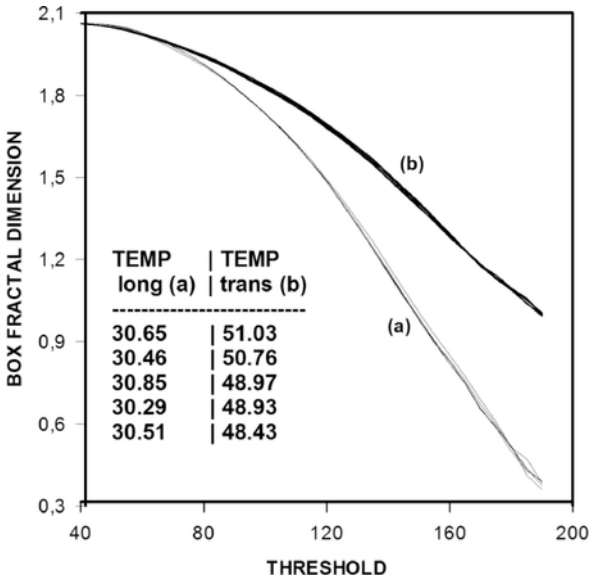

Fig. 11. BFDC and the corresponding "fractal temperatures" T^* for Rugotest experiment: a) five curves in the longitudinal direction; b) five curves in the transversal direction. Notice that in both cases the curves mostly overlap.

TM-6CN (CCIR Standard, interlaced scanning, pixel size 8.6 μm × 8.3 μm), connected to a personal computer with a frame grabber was used to record the images, which were digitized to 256 intensity levels. The speckles were well resolved by the CCD sensor and the average intensity of the laser was maintained constant. The displacement of a ground glass diffuser was performed by using an Aerotech ARS 302MM stepping motor (2 μm per step).

As the image of each step of the motor is a static frame, the dynamic case is simulated by adding and averaging pairs of frames. The different velocities of dynamic speckles were simulated using pairs of frames separated by different numbers of steps.

The BFD method was applied and then we used Eq. (3) to calculate the best numerical fit function using the Fermi–Dirac equation. Each fit was characterized by a "fractal temperature" equivalent that describes the rate of change of the box fractal curve.

Fig. 12a) shows the results of the controlled step motor experiments in translation condition (in dot symbols) and the theoretical curve obtained using the Fermi–Dirac equation in a continuous line. We presented two examples, for frames separated by 35 steps (curve (a)) and for frames separated by 90 steps (curve (b)) Also in this case, it can be seen that the points can be suitably adjusted, with the fractal curve showing a very good agreement between them ($r^2 = 0.99752$ for curve (a) and $r^2 = 0.99547$ for curve (b)).

Fractal temperature T^* follows a continuous decreasing behavior as shown in Fig. 12b) for experimental measurements, and is stabilized after reaching a high enough activity value. In the experimental curve it can be seen that the temperature initially changes slowly with increased activity. Then a fast change region follows where the temperature diminishes until a stabilization region is reached at the lower temperature value. The increase in activity appears as a lowering in the temperature T^*.

3.2.2. Drying of paint experiment

We tested the BFDC algorithm in a well-known dynamic speckle experiment, the process of drying of paint [20].

In this case, an attenuated unexpanded 10 mW He–Ne laser was used to illuminate the sample. A lensless CCD camera (Pulnix TM-6CN), connected to a personal computer with a frame grabber was used to record the images, which were digitized to 256 intensity levels (8 bits). The speckles were well resolved by the CCD sensor and the average intensity of the laser was maintained constant.

Paint was applied horizontally in a 75 μm thick film. The film was prepared on 4 × 4 cm^2 glass substrate using a standard drawdown stainless steel applicator onto a flat substrate. In this way, a film with a flat level surface was obtained.

We registered eight series of 400 images of dynamic objective speckles of 200 × 200 pixels size with 30 min drying lapses between them. Each one of these series was assumed to represent a different state of drying. We labeled them with a number that indicates the time in minutes at which they were registered. Time 0 ($t = 0$) is the instant of application of the paint.

The BFDC algorithm was applied to the frames in different drying paint states processed using 5 boxes.

Then, we calculated the best numerical fit function using the Fermi–Dirac equation (Eq. (3)). Each fit was characterized by a "fractal temperature" T^* equivalent that describes the rate of change of the box fractal curve.

Fig. 13a) shows the experimental results (in dot symbols) and the theoretical curve obtained using the Fermi–Dirac equation in a continuous line. It can be seen that the experimental points show the fractal curves in the extreme cases: a) wet paint at the initial time ($t = 0$) and b) dry paint at the end of the process ($t = 210$ min). Experimental points can be suitably adjusted, with the fractal curve showing a very good agreement between them: a) $r^2 = 0.999055$, b) $r^2 = 999{,}565$.

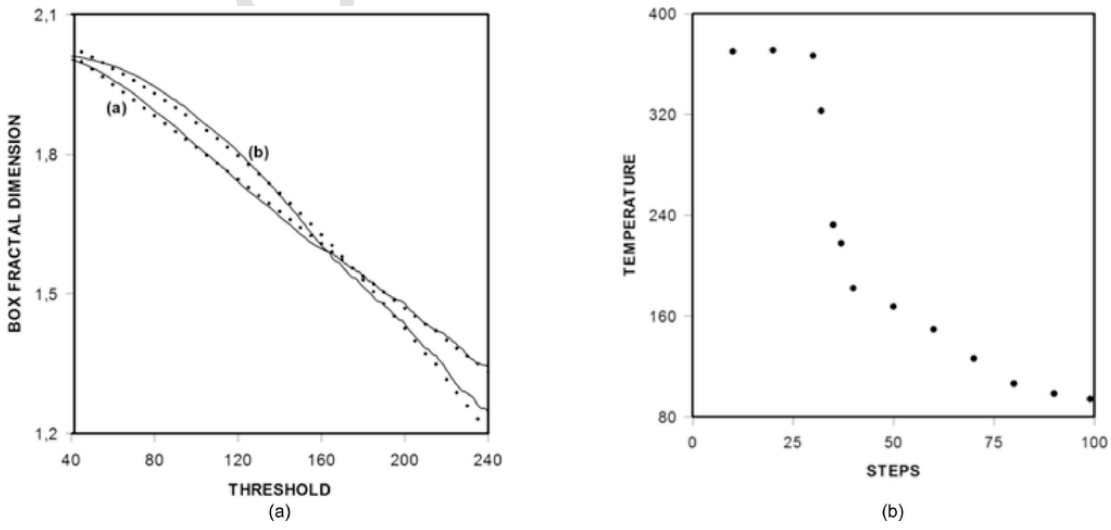

Fig. 12. Experimental step motor: a) in dots measured values and in continuous line the Fermi–Dirac calculated value; (a) frames separated by 35 steps, (b) frames separated by 90 steps. b) "fractal temperatures" T^*.

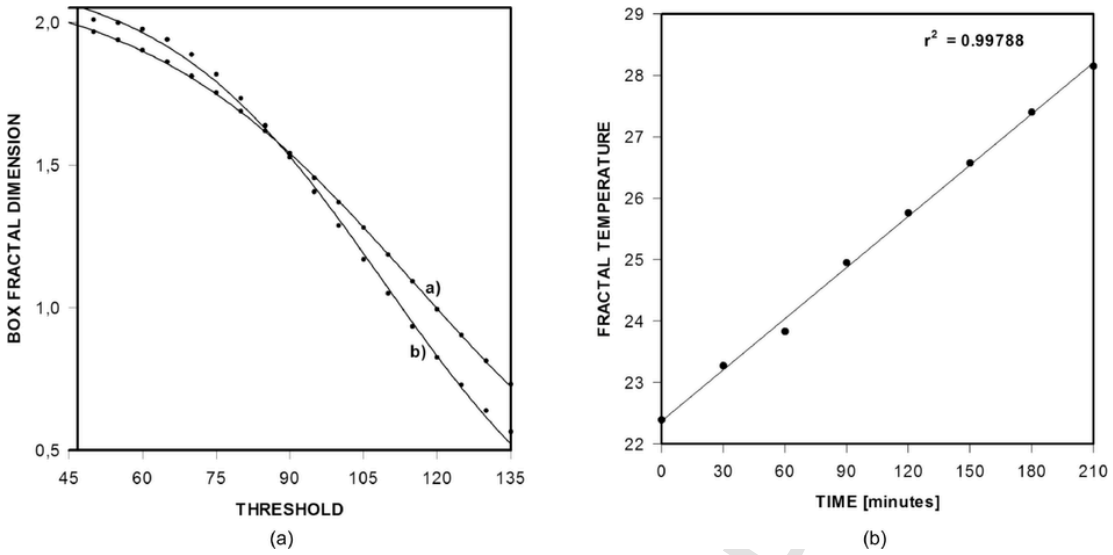

Fig. 13. In a) paint drying process: in dots measured values and in continuous line the Fermi–Dirac calculated value; a) wet paint; b) dry paint. In b) paint drying process: "fractal temperature" T^*.

The fractal temperatures T^* obtained from the numerical fit of the former are shown in Fig. 13b) for every state of drying. Note that, unlike the step motor cases, the temperature curve must be growing as the drying progresses. In this case, the speckle pattern activity diminished with time. In the final stage of the process (dry paint) there is no activity. As expected, we obtain a monotonically increasing curve showing the progressive drying process from the wettest to the dry paint situation where it stabilizes when the drying is complete. Experimental points can be linearly fitted, showing a very good agreement ($r^2 = 0.99788$).

3.2.3. *Speckle in ultrasound images*

Ultrasound images show speckle phenomena. We tested the BFDC and its derivative in two ultrasound images of thyroids (downloaded from the web) classified as healthy and pathologic.

Fig. 14 shows the fractal curves: a) healthy case, b) pathologic case.

Fig. 15 shows the derivatives for: a) healthy case, b) pathologic case. In the first case the derivative shows a single broad noisy lump. In the second case, the minimum of the lump is reduced by about a half and for higher thresholds there appears a noticeable structure in the derivative of the fractal curve, showing the presence of a different texture.

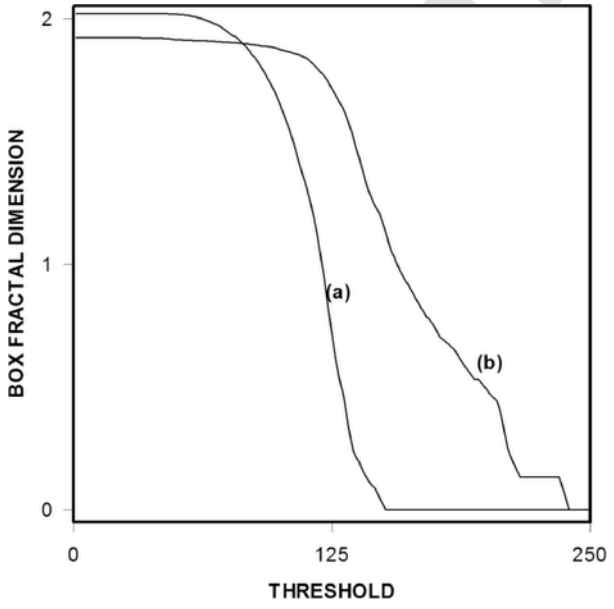

Fig. 14. BFDC of ultrasound images of thyroids: a) healthy case, b) pathologic case.

These results are shown as purely illustrative examples and do not imply its possible use as a diagnostic tool. In that case, a systematic statistical validation procedure would be required.

4. Conclusions

We propose a box fractal dimension algorithm that, unlike other algorithms, can be used in a wide set of applications, such as in incoherent illuminated ordinary images and in controlled, static and dynamic speckle cases.

We have shown that the procedure to calculate the BFD can be extended to obtain a curve that is versatile and useful for the characterization of some aspects of the dynamics of speckle. Nevertheless, as the fractal dimension has been found useful for different types of textures, the concept could be adapted for treating other types of images. In principle, the procedure could be tested in many of the numerous applications that have been found for fractal dimensions in general.

As an example, we showed how the proposed approach was applied to the classic mandrill image.

It was found that in some cases the BFDC could be approximated by a mathematical expression and an analogue to temperature used to characterize its time evolution. Then we presented a formalism of the fractal box dimension curve as a descriptor of the speckle pattern images in both static and dynamic cases. We showed its potential usefulness using some examples such as controlled experiments, industrial applications (surface roughness and polymer drying) and a biological case (ultrasound images).

Other applications are currently being investigated, but the results are still preliminary and a careful validation is needed for any cases. Work is continuing to refine the research methodology and to perform comparative studies with other algorithms.

Application of the box fractal to segment activity speckle images in several situations will be reported elsewhere.

Acknowledgments

This work was supported by the Faculty of Engineering, UNLP, CONICET and CICPBA, Argentina.

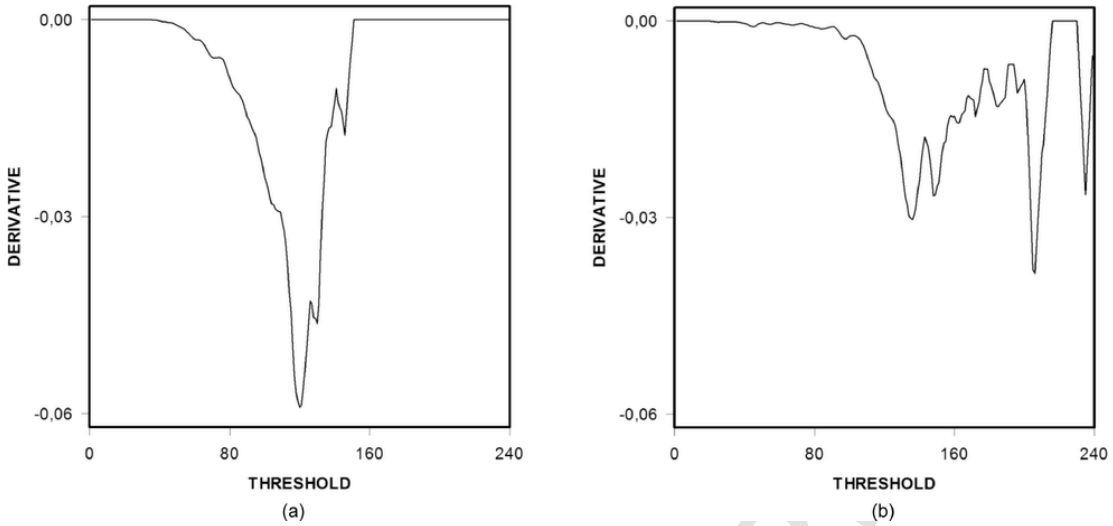

Fig. 15. Derivatives of BFDC of ultrasound images of thyroids: a) healthy case, b) pathologic case.

References

[1] (Ed.), in: J.C. Dainty (Ed.), Laser speckle and related phenomena, Springer Verlag, Berlin-New York, 1975.

[2] J.W. Goodman, Speckle phenomena in optics: theory and applications, Roberts & Company, Englewood, CO, 2007.

[3] F. Perez-Quintian, M. Rebollo, E.N. Hoggert, M.R. Landau, N.G. Gaggioli, Relationship between speckle correlation and refraction index variations: applications for roughness measurements, Opt. Eng. 35 (4) (1996) 1175.

[4] (Ed.), in: P.K. Rastogi (Ed.), Digital speckle pattern interferometry and related techniques, Wiley-VCH, 2000.

[5] (Eds.), in: H. Rabal, R. Braga (Eds.), Dynamic laser speckle and applications, CRS Press, Taylor and Francis, Boca Raton, FL, 2009.

[6] A.L. Dai Pra, L.I. Passoni, G.H. Sendra, M. Trivi, H.J. Rabal, Signal feature extraction using granular computing. Comparative analysis with frequency and time descriptors applied to dynamic laser speckle patterns, Int J Comput Intell Syst 8 (2015) 28–40, Suppl 2.

[7] E.E. Grumel, N. Cap, A. Longarzo, H. Rabal, M. Trivi, The fractal dimension curve as a descriptor of biospeckle images, in: H. Michinel (Ed.), Proceedings of XXIII general congress international commission for optics (ICO-23), 2014, (Ed.), Opt_Imag_106_157.

[8] B.B. Mandelbrot, The fractal geometry of nature, W. H. Freeman and Co, 1982.

[9] N. Otsu, A threshold selection method from gray-level histograms, Trans Syst Man Cybern 9 (1979) 62–66.

[10] B. Chaudhuri, N. Sarkar, An efficient approach to compute fractal dimension in texture image, Pattern Recognit 25 (9) (1992) 035–1041.

[11] B. Chaudhuri, N. Sarkar, Texture segmentation using fractal dimension, IEEE Trans Pattern Anal Mach Intell Pap 17 (1) (1995) 72–77.

[12] J Li, Q Du, C. Sun, An improved box-counting method for image fractal dimension estimation, Pattern Recognit. Pap. 42 (11) (2009) 2460–2469.

[13] YU Liu, L Chen, H Wang, et al., An improved differential box-counting method to estimate fractal dimensions of gray-level images, J Visual Commun Image Represent. Pap 25 (5) (2014) 1102–1111.

[14] CC Li, LF Cheng, T He, L Chen, F Yu, et al., ``An improved differential box-counting method of image segmentation", SPIE, 2016.

[15] W.K. Pratt, Digital image processing, John Wiley and Sons, 1978.

[16] J.W. Goodman, Laser speckle and related phenomena (Ed.), in: J.C. Dainty (Ed.), Springer Verlag, Berlin-New York, 1975, Chap. 2.

[17] R. Eisberg, R. Resnick, Quantum physics, John Wiley & Sons, 1985.

[18] G.H. Sendra, H.J. Rabal, M. Trivi, R. Arizaga, Numerical model for simulation of dynamic speckle reference patterns, Opt Commun 282 (2009) 3693–3700.

[19] T. Okamoto, T. Asakura, The statistics of dynamic speckles (Ed.), in: E. Wolf (Ed.), Progress in optics, 34, North Holland, Amsterdam, 1995.

[20] J. Amalvy, C. Lasquibar, R. Arizaga, H.J. Rabal, M. Trivi, Application of dynamic speckle interferometry to the drying of coatings, Prog Org Coat 42 (2001) 89–99.